Rapid #: -22132219

CROSS REF ID: **1128191**

LENDER: **ATUNB (University of Notre Dame Australia Broome Library) :: Broome Library**

BORROWER: **WTU (Washington University in St. Louis) :: Olin Library**

TYPE:	Article CC:CCG
JOURNAL TITLE:	Cerebral cortex
USER JOURNAL TITLE:	Cerebral cortex (New York, N.Y. 1991)
ARTICLE TITLE:	Functional parcellation of the neonatal cortical surface.
ARTICLE AUTHOR:	Myers, Michael J
VOLUME:	34
ISSUE:	2
MONTH:	
YEAR:	2024-01
PAGES:	-
ISSN:	1047-3211
OCLC #:	

Processed by RapidX: 2/26/2024 10:01:20 PM

OXFORD

Cerebral Cortex, 2024, **34**, bhae047
https://doi.org/10.1093/cercor/bhae047
Advance access publication date 17 February 2024
Original Article

Functional parcellation of the neonatal cortical surface

Michael J. Myers[1,†], Alyssa K. Labonte[1,2,†,*], Evan M. Gordon[3], Timothy O. Laumann[1], Jiaxin C. Tu[2,3], Muriah D. Wheelock[3], Ashley N. Nielsen[1], Rebecca F. Schwarzlose[1], M. Catalina Camacho[1], Dimitrios Alexopoulos[4], Barbara B. Warner[5], Nandini Raghuraman[6], Joan L. Luby[1], Deanna M. Barch[1,7], Damien A. Fair[8,9,10], Steven E. Petersen[3,4], Cynthia E. Rogers[1], Christopher D. Smyser[3,4,5], Chad M. Sylvester[1,3,11]

[1]Department of Psychiatry, Washington University in St. Louis, St. Louis, MO 63110, United States,
[2]Neurosciences Graduate Program, Washington University in St. Louis, St. Louis, MO 63110, United States,
[3]Department of Radiology, Washington University in St. Louis, St. Louis, MO 63110, United States,
[4]Department of Neurology, Washington University School of Medicine, St. Louis, MO 63110, United States,
[5]Department of Pediatrics, Washington University School of Medicine, St. Louis, MO 63110, United States,
[6]Department of Obstetrics and Gynecology, Washington University School of Medicine, St. Louis, MO 63110, United States,
[7]Department of Psychological & Brain Sciences, Washington University in St. Louis, St. Louis, MO 63110, United States,
[8]Masonic Institute for the Developing Brain, University of Minnesota, Minneapolis, MN 55414, United States,
[9]Institute of Child Development, University of Minnesota, Minneapolis, MN 55455, United States,
[10]Department of Pediatrics, University of Minnesota, Minneapolis, MN 55454, United States,
[11]Taylor Family Institute for Innovative Psychiatric Research, Washington University School of Medicine, St. Louis, MO 63110, United States
*Corresponding author: Department of Psychiatry, Washington University, 660 S. Euclid, Campus Box 8511, St. Louis, MO 63110, United States. Email: alabonte@wustl.edu
[†]Michael J. Myers and Alyssa K. Labonte contributed equally to this work.

The cerebral cortex is organized into distinct but interconnected cortical areas, which can be defined by abrupt differences in patterns of resting state functional connectivity (FC) across the cortical surface. Such parcellations of the cortex have been derived in adults and older infants, but there is no widely used surface parcellation available for the neonatal brain. Here, we first demonstrate that existing parcellations, including surface-based parcels derived from older samples as well as volume-based neonatal parcels, are a poor fit for neonatal surface data. We next derive a set of 283 cortical surface parcels from a sample of $n = 261$ neonates. These parcels have highly homogenous FC patterns and are validated using three external neonatal datasets. The Infomap algorithm is used to assign functional network identities to each parcel, and derived networks are consistent with prior work in neonates. The proposed parcellation may represent neonatal cortical areas and provides a powerful tool for neonatal neuroimaging studies.

Key words: cortical areas; fMRI; functional connectivity; neonate; parcellation.

Introduction

The cerebral cortex is composed of discrete yet interconnected cortical areas that are fundamental macroscale units of the central nervous system. Cortical areas can be defined as contiguous portions of cortex which are distinguished from their neighbors by abrupt changes in function, architectonics, connectivity, and topography (FACT) (Sejnowski and Churchland 1989; Felleman and Van Essen 1991). Sets of highly interconnected cortical areas, in turn, comprise functional networks that support different aspects of cognition and constitute a higher level of brain organization (Petersen and Sporns 2015). An important goal of human neuroscience is to identify and characterize these cortical areas and functional networks.

"Parcels" are subdivisions of the cortex derived empirically in neuroimaging studies based on abrupt transitions in patterns of functional connectivity (FC) across the cortical surface (Cohen et al. 2008; Wig et al. 2014; Gordon et al. 2016). These abrupt transitions in FC may reflect differences between adjacent cortical areas in function and connectivity (Gordon et al. 2016), two of the four FACT criteria, suggesting that parcels could represent cortical areas. Progress has been made in utilizing this method to generate sets of parcels that cover the cortical surface ("parcellations") in older infants and adults (Glasser et al. 2016; Gordon et al. 2016; Schaefer et al. 2018; Wang et al. 2023), and studies using these parcellations have generated a wealth of knowledge regarding adult human brain architecture, function, and relations to individual differences in behavior (Wig et al. 2014; Laumann et al. 2015; Gordon et al. 2017; Han et al. 2018; Shine et al. 2019; Sydnor et al. 2021).

Despite the developmental, ontogenetic, and clinical significance of neonatal brain organization, neonatal cortical areas have not been systematically characterized. To date, there are no standard neonatal cortical surface parcellations based on transitions in FC as there are for older infants and adults. Past approaches dividing the neonatal brain into functionally relevant subdivisions have used volume-based rather than surface-based analyses (Scheinost et al. 2016; Shi et al. 2017). The suitability of these volume-based parcels for surface-based analyses and their relation to cortical areas is unclear. Further, adult parcellations are unlikely to fit neonatal data because of the non-linear and non-uniform cortical expansion that takes place over development (Hill et al. 2010; Li et al. 2013).

Received: November 18, 2023. **Revised:** January 23, 2024. **Accepted:** January 26, 2024

The lack of knowledge of neonatal cortical areas is a significant gap, as the neonatal period is a landmark stage in neural development that serves as a starting point for postnatal experience-dependent learning (Rai et al. 2022). A characterization of the number, locations, and network assignments of neonatal cortical areas is needed to advance our understanding of typical and atypical brain development. A neonatal surface parcellation would also provide a valuable tool for neonatal neuroimaging studies, enabling researchers to reduce dimensionality, increase power by averaging signals over homogeneous regions of cortex, reduce problems of multiple comparisons, and increase methodological consistency across studies and research groups (Wig et al. 2011).

Part of characterizing cortical areas in neonates includes a description of their functional network organization. Functional networks represent a higher level of brain organization and can be defined based on sets of highly interconnected cortical areas or parcels (Petersen and Sporns 2015). Because of the weak long-range anterior–posterior FC of neonates, most prior work describes neonatal networks as anatomically isolated chunks of cortex rather than the distributed organization characteristic of adults (Fransson et al. 2007, 2009; Gao et al. 2009, 2013, 2015, 2017; Doria et al. 2010; Smyser et al. 2010, 2016; De Asis-Cruz et al. 2015; van den Heuvel et al. 2015; Keunen et al. 2017; Sylvester et al. 2022). An important goal of developmental systems neuroscience is to characterize the network "identities" of individual neonatal parcels and track the evolving network relations of these parcels over development. Such a description would inform the evolving function of cortical areas over development and provide a foundation for studies of typical and atypical development.

In the current study, we derived a set of neonatal cortical surface parcels based on abrupt differences in FC across the cortical surface in a sample of $n = 261$ neonates. To test the reliability of the parcellation, we split neonates with the most data (primary generation dataset; $n = 131$) into two halves, generated parcellations from each half, and then tested each parcellation on the held-out half of the data. To ensure the generalizability of our parcellation, we then validated it in three external datasets. Finally, we clustered the derived parcels into neonatal functional brain networks. Results provide a robust surface-based neonatal parcellation, uncover putative neonatal cortical areas, reveal properties of neonatal brain network organization, and have practical utility for neonatal neuroimaging studies. The derived parcellation (the "Myers-Labonte Parcellation") and the code used to derive the parcels is publicly available for use at https://github.com/myersm0/WatershedParcellation.jl/.

Materials and methods

This study was approved by the Human Research Protection Office at Washington University in St. Louis. All mothers of neonatal participants provided informed consent prior to study initiation. The primary dataset in this study, Early Life Adversity and Biological Embedding (eLABE), has been recently described (Lean et al. 2022; Nielsen et al. 2022; Sylvester et al. 2022). The current study focused on fMRI data collected from 261 healthy, full-term neonates (average postmenstrual age (PMA) 41.3 wk, range 38–45; Table 1) from the eLABE dataset scanned between September 2017 and March 2020.

Primary dataset

Neuroimaging was performed in full-term neonates during natural sleep using a Siemens 3T PRISMA scanner and 64-channel infant specific head coil. Prior to scanning, neonates were fed, swaddled, and positioned in a head-stabilizing vacuum fix wrap (Mathur et al. 2008). A T2-weighted image (sagittal, 208 slices, 0.8-mm isotropic resolution, time to echo (TE) = 563 ms, tissue T2 = 160 ms, repetition time (TR) = 3200 ms) was collected. Functional imaging (fMRI) was performed using a BOLD gradient-recalled echo-planar multiband (MB) sequence (72 slices, 2.0-mm isotropic resolution, TE = 37 ms, TR = 800 ms, MB factor = 8). Using the same parameters, spin-echo field maps were also obtained. Depending on tolerability of the scan, between 2 and 9 fMRI BOLD scans were acquired for each neonate (mean 3.75 runs). Runs were 420 frames, ~5.6 min in length, and were collected in both the anterior-to-posterior (AP) and posterior-to-anterior (PA) direction; a typical scan session included 2 AP runs and 2 PA runs. AP and PA scans were concatenated following fMRI preprocessing, but prior to FC processing. Framewise integrated real-time MRI monitoring (FIRMM) was used during scanning to monitor real-time neonate movement (Dosenbach et al. 2017; Badke et al. 2022).

Validation datasets

Several independent datasets were used to validate results. Each dataset comes from studies that were approved by the Human Research Protection Office at Washington University in St. Louis. The first validation set, CUDDEL+OXYGEN, is a combination of two datasets, Prenatal Cannabis Use and Development of Offspring Brain and Behavior During Early Life (CUDDEL) and Maternal Oxygen in Labor (OXYGEN), both identical to the primary dataset (eLABE) in recruitment methods, demographics, neuroimaging acquisition, and processing. CUDDEL is enriched for mothers who reported cannabis use during pregnancy, and 33% of the cohort used in these analyses were exposed to cannabis in-utero. OXYGEN recruited mothers during labor with the goal of scanning healthy neonates within the first 72-h of life. As both CUDDEL and OXYGEN were ongoing studies during the time of our analyses, we restricted our use of the data to the sample sizes that were available at the start of these analyses ($n = 36$ and $n = 5$, respectively). Supplementary Fig. 1 shows that we obtained robust results with these sample sizes.

A second validation dataset, Precision Baby (PB003), consists of a single neonate (Male; 44-wk PMA) scanned across five consecutive days for a total of 3.27 h of low-motion fMRI data (FD < 0.25). Recruitment of this neonate was the same as the primary dataset (eLABE), and neuroimaging acquisition and processing were also largely similar. A T2-weighted was collected using the same parameters as the primary dataset and was used to align functional data across all scan sessions for each neonate. fMRI was performed using a BOLD gradient-recalled echo-planar multiband sequence (60 slices, 2.4-mm isotropic resolution, TE = 37 ms, TR = 1,200 ms, MB factor = 4). Using the same parameters, spin-echo field maps were also obtained.

The third external validation dataset, WUNDER, consists of 70 full-term neonates scanned between 2007 and 2016, and has been previously described (Smyser et al. 2010). Neuroimaging for this dataset was performed during natural sleep using a Siemens 3 T TRIO scanner and infant-specific head coil. Structural images were collected with a turbo spin-echo T2-weighted sequence (TE = 160 ms, TR = 8,600 ms, 1 mm isotropic resolution). fMRI was performed using a gradient-echo echo planar image sequence sensitized to T2* BOLD signal changes (2.4 mm isotropic resolution, TE = 28 ms, TR = 2,910 ms). Spin-echo field maps were also obtained using the same parameters. A total of 200 frames were collected over 10 min for each run. A minimum of one run was required for inclusion, but some infants had up to four runs.

Table 1. Full primary dataset demographics table.

Neonatal characteristics ($n = 261$)	***n***	**Mean**	**SD**
Sex			
Male	141		
Female	120		
Gestational age at birth (weeks)		38.5	1.0
Postmenstrual age at scan (weeks)		41.3	1.3
Birthweight in grams		3274.0	489.9
Area deprivation index		67.9	24.9
Child's race			
African American	158		
White	101		
Chinese	3		
Other Pacific Islander	1		
Other	1		
Ethnicity			
Hispanic	6		
Non-Hispanic	253		
Unspecified	2		
Neonatal fMRI Characteristics	***n***	**Mean**	**SD**
fMRI data collected (minutes)		19.1	5.2
fMRI data retained (minutes)		16.6	4.4

fMRI preprocessing

All datasets underwent identical preprocessing and FC processing except WUNDER, which is described below.

fMRI preprocessing included correction of intensity differences attributable to interleaved acquisition, linear realignment within and across runs to compensate for rigid body motion, bias field correction, intensity normalization of each run to a whole-brain mode value of 1000, distortion correction, and linear registration of BOLD images to the adult Talairach isotropic atlas (Talairach and Tournoux 1988) using in-house software (ftp://imaging.wustl.edu/ pub/raichlab/4dfp_tools/). Field distortion correction was performed using the FSL TOPUP toolbox (http://fsl.fmrib.ox.ac.uk/fsl/fslwiki/TOPUP). BOLD images for each subject were registered as follows: BOLD → individual T2 → cohort-specific T2 atlas → 711-2 N Talairach atlas (adult space). The cohort-specific T2 atlas was created from a subset of 50 neonates from the eLABE dataset.

The volumetric preprocessed BOLD data were then mapped to subject-specific surfaces prior to FC-processing. The Melbourne Children's Regional Brain Atlases (MCRIB) (Alexander et al. 2017; Adamson et al. 2020), a surface-based neonatal tissue segmentation approach, was used to generate surfaces for each subject from their T2 image following linear transformation to adult Talairach (711-2 N) space. One subject in the held-out half of the dataset ($n = 130$), which was not used to generate the Myers-Labonte parcellation, did not have a T2-weighted image, but instead had a T1-weighted image which was utilized to generate a faux T2-weighted image for segmentation and surface reconstruction with MCRIB. Subject-specific surfaces were aligned across subjects into the "fsLR_32k" surface space using spherical registration procedures (Glasser et al. 2013) adapted from the Human Connectome Project as implemented in Connectome Workbench 1.2.3 (Marcus et al. 2011, 2013). All volumetric and surface registrations were visually inspected to ensure accuracy. Additional information regarding surface reconstruction can be found in the Supplemental Materials.

Following initial preprocessing and surface reconstruction and registration to fsLR_32k space with a small smoothing kernel ($\sigma = 1$ mm), BOLD time series were censored at framewise displacement (FD) < 0.25 mm, and only epochs of at least 3 consecutive frames with FD < 0.25-mm were included. A minimum of 10 min (750 frames) of usable data were required from each subject for inclusion. This data then underwent FC processing as follows (Power et al. 2014; Gordon et al. 2016): (i) demean and detrend within each run, ignoring censored frames; (ii) multiple regression with nuisance time series including white matter, ventricles, and whole brain (average gray matter signal), as well as 24 parameters derived from head motion, ignoring censored frames. Finally, retained data were interpolated at censored timepoints to allow band-pass filtering (0.005 Hz < f < 0.1 Hz).

Time courses for surface data were smoothed with geodesic 2D Gaussian kernels after FC processing ($\sigma = 2.25$ mm). FC was computed as the Fisher z-transformed Pearson correlation between time courses from pairs of surface parcels or vertices, as detailed below.

In contrast to the other datasets, BOLD and FC pre-processing in the WUNDER dataset was done in volume-space as has been previously described (Smyser et al. 2010; Herzmann et al. 2019). Key differences in FC processing from the other datasets included low-pass filtering (<0.08 Hz) rather than band-pass filtering; and the timeseries for the white matter and CSF nuisance regressors were obtained from hand-drawn samples of these areas rather than automated segmentations. Following FC processing, data were mapped to each individual's surface in fs_LR32k space and then spatially smoothed ($\sigma = 4.1$ mm). These spatially smoothed surface-aligned timeseries were used for computing FC. Only subjects having at least 5 min of low-motion fMRI data were included in the analysis; this more lenient threshold was allowed for the older WUNDER dataset to include as many subjects as possible in the group average.

Boundary map generation

Following the notion that adjacent cortical areas should be separated by abrupt changes in function and connectivity (Felleman and Van Essen 1991), the method described in (Gordon et al. 2016)

was used to identify transitions in FC across the cortical surface. First, pairwise FC of all ∼60k cortical surface vertices was computed for each subject, resulting in a 60k × 60k square resting state functional connectivity (RSFC) matrix where each row or column is the "correlation map" of a particular vertex: a vector of values characterizing a single vertex's correlation with all other vertices. Next, a 60k × 60k "similarity matrix" was generated for each subject as the pairwise correlations between all the correlation maps; the similarity matrix thus represents how similar the correlation maps are between every possible pair of vertices. The first spatial derivative of each subject's similarity matrix was then computed, producing a 60k × 60k matrix in which each column is the "gradient map" of a particular vertex, representing how abruptly that vertex's similarity in RSFC with other vertices changes as one moves across the cortex. Vertex-wise gradient maps were then averaged across all subjects, creating an across-subjects average gradient map for each vertex, and smoothed with a kernel of $\sigma = 2.55$ mm. The watershed algorithm (Beucher and Lantuejoul 1979) was applied to each vertex's average gradient map. With this method, regions are "filled up" from their local minima (low points in the gradient map) until they reach border vertices that could be assigned to more than one region; such borders represent locations of peak spatial gradient (i.e. rapid changes in FC similarity) across participants. We experimented with a parameter to control the number of bins into which continuous-valued heights are discretized for iteration within the watershed algorithm. In the original algorithm outlined for adults in (Gordon et al. 2016), this steps parameter was set to 400 bins to improve computation time; however, noting that higher values of this parameter (i.e. smaller bins for each iteration of the watershed) produced sharper edge maps in our dataset, we modified this parameter to 1,600 bins. This parameter was also modified and set to 1,600 to recompute the adult boundary maps from Gordon et al. (2016) to show fair comparisons between adults and neonates. The binary maps of gradient peaks (borders) were then averaged across all gradient maps to produce a "boundary map," which represents the probability of each particular vertex being classified as a border. A flowchart of this method can be seen in Supplementary Fig. 2. Adult and neonatal boundary maps were compared with a smoothness metric using a built-in Connectome Workbench command (wb_command -cifti-estimate-fwhm).

Parcel generation

Parcels were generated using the same watershed procedure described above to fill the boundary map from its local minima. Several parameters can influence the sizes and shapes of the resulting parcels. One of these parameters concerns the tendency for two neighboring parcels to be combined into one parcel. Two neighboring parcels may be combined into a single parcel if a relatively small boundary between them suggests that their respective connectivity patterns are not sufficiently different. To select an appropriate value for this parameter, we visually inspected a range of thresholds (from 0.25 to 0.4) and chose the value (0.38) that best respected the salient boundaries we observed in the boundary map.

The second parameter concerns the height at which we stopped "filling" the regions, the height criterion. In the original method outlined for adults in (Gordon et al. 2016), this value was selected as the 90th percentile of all height values, such that the 10% of vertices exceeding this height were left unassigned (i.e. not belonging to any parcel). These unassigned values may be considered transitional zones in which the connectivity is rapidly changing. This parameter determines the approximate percentage of the cortex that is to be covered by the parcellation. We tested several thresholds for this height criterion parameter, ranging from the 25th to 90th percentiles (see Fig. 4). The highest homogeneity of the parcels in external datasets was observed using the 50% height threshold. Thus, this threshold was used to generate the parcellation used for all subsequent analyses.

The "final" parcellation was generated using the procedure above in the primary dataset, the half of subjects with the most data following frame censoring ($n = 131$). This restriction ensured that the parcellation was generated from subjects with data with the lowest noise, as well as to test the parcellation in the held-out half of the as described in the results ("Parcellation generated from neonatal data has high homogeneity in external datasets"). This procedure resulted in 304 parcels tiling the cortical surface, 153 parcels in the left hemisphere and 151 parcels in the right. Parcels with fewer than 15 vertices outside of the low signal areas (mean signal <750 after mode 1,000 normalization) (Ojemann et al. 1997; Gordon et al. 2016) were removed because they were unlikely to be reliable. This procedure removed 22 parcels primarily in the inferior temporal and orbito-frontal lobes, resulting in 282 parcels tiling the cortical surface. We also identified four parcels that did not appear biologically plausible because of their shapes. Parcel #217 was trimmed. One parcel with a biologically implausible shape was split into two parcels (#4, #137). We removed one vertex from parcel #33. We added two vertices to parcel #121 to fill in a hole in the middle. The resulting final Myers-Labonte Parcellation consisted of 283 parcels, with 146 parcels in the left hemisphere and 137 in the right.

Parcel homogeneity

The parcel generation procedure outlined above creates parcels based on distinct boundaries which indicate differences in FC patterns among adjacent cortical regions (Gordon et al. 2016). These generated parcels should both be distinct from neighboring parcels in connectivity and show homogenous connectivity within each parcel. To measure the homogeneity of a parcel, a principal components analysis (PCA) is run in which the inputs are the connectivity patterns from all the individual vertices comprising a parcel in the group average data. Following (Gordon et al. 2016), we define homogeneity as the percent of variance explained by the first component.

Homogeneity is highly related to the size of a parcel such that smaller parcels tend to have higher homogeneity than larger parcels (Gordon et al. 2016; Arslan et al. 2018). To provide a fair point of comparison, we considered a null distribution of random parcellations having parcels of the same sizes and shapes, and in the same configuration as our true parcellation, but randomly relocated about the cortical surface. To do this, we replicate the rotation method described in (Gordon et al. 2016). Briefly, the original parcellation was randomly rotated around each of the x, y, and z axes on a spherical expansion of the cortical surface, allowing for the random relocation of each parcel while maintaining their size, shape, and relative positions to one another. This rotation procedure was repeated 1,000 times, whereby each hemisphere was rotated symmetrically with each iteration. The average homogeneity of the original parcellation (described above) was then compared with the homogeneity values of each of the randomly rotated parcellations, calculated as a z-score [(original homogeneity—mean of random homogeneities)/standard deviation of random homogeneities].

Parcel reliability

To test the reliability of our parcellation, we randomly split the primary dataset ($n = 131$) in half, generated parcellations from each half separately, and evaluated the overlap of resulting parcels. To quantify the spatial overlap, the Dice similarity coefficient (DSC) was computed on binarized parcel identity maps for the two halves. To assess the significance of this result, we randomly rotated both parcellations 1,000 times (previously described in detail under "Parcel Homogeneity"), each time computing the DSC of the two randomly rotated parcellations to derive a null distribution against which to compare the value obtained in the true parcellations.

Identification of parcel network structure

The community detection algorithm Infomap was used to empirically derive functional brain networks from our parcels (Rosvall and Bergstrom 2008; Power et al. 2011). For each subject in the primary dataset, we created a parcellated time series by calculating the mean within-parcel time series over each of the 283 parcels. We then cross-correlated these parcellated time series to generate a parcel-wise correlation matrix. Parcel-wise correlation matrices were Fisher z-transformed and averaged across all subjects to generate a single parcel-wise correlation matrix, which was then masked to remove functional connections with a distance <30 mm along the cortex between the nearest vertices of each pair of connected parcels. Functional connections surviving this distance threshold were then binarized to isolate only the strongest positive connections over a range of thresholds chosen to achieve varying degrees of sparseness (in 40 steps ranging from 0.25% to 10%). The resulting 40 connection matrices were then used separately as inputs to the Infomap algorithm, to assign parcels to communities (or networks) based on the maximization of within-community random walks in the connection matrix. This produced 40 network solutions, one for each of the edge densities.

Putative network identities were then assigned by matching communities at each threshold to a set of previously described neonate-specific vertex-wise networks (Supplementary Fig. 3) [from the 1.25% edge density vertex-wise Infomap solution as illustrated in Fig. 3A in (Sylvester et al. 2022)]. This matching approach proceeded as follows. At each density threshold, all identified communities were compared (using spatial overlap, quantified with the Jaccard index) to each of the networks in turn. The best-matching (highest-overlap) parcel-wise community was assigned that network identity; that community was not considered for comparison with other networks within that threshold. Matches lower than Jaccard = 0.1 were not considered (to avoid matching based on only a few vertices). Matches were first made with larger networks (Anterior and Posterior Default, Lateral Visual, Motor, Fronto-Parietal, Dorsal Attention), and then to the smaller networks (Orbito-Frontal and Premotor). A "consensus" network assignment was then derived by collapsing assignments across thresholds, giving each parcel the assignment it had at the sparsest possible threshold by which it was successfully assigned to one of the known networks.

A few manual modifications were made to the "consensus" network assignments, which were evident in Infomap solutions, but that did not appear in the neonate-specific vertex-wise network template used in the consensus procedure described above. The motor network, which appeared as a single network in the template, was divided into motor hand and motor mouth networks, based on assignments at the sparest edge threshold (0.25%). Further, parcel number 161 was changed from the lateral visual to the medial visual network, based on the network that had been assigned at sparser edge densities rather than the assignment from the consensus algorithm described above. This decision was made based on the overall pattern across edge densities. Brain surface visualizations were generated in Julia version 1.8.3 with the Makie plotting library (Danisch and Krumbiegel 2021).

Spring-embedded plots were also generated to visualize how clustering patterns of parcels changed across various edge densities. All plots were generated using the igraph library in R (Nepusz 2006).

Results

Performance of adult and infant parcels on neonatal data

We first investigated how well surface-based parcels generated from adults and older infants, as well as neonate-specific volume-based parcels, performed on our neonatal data. Publicly available surface-based adult (Glasser et al. 2016; Gordon et al. 2016; Schaefer et al. 2018) and older-infant parcellations (Wang et al. 2023), as well as neonate-specific volume-based parcellations (Scheinost et al. 2016; Shi et al. 2017) were tested on the half of the dataset which was not used to generate the neonatal parcellation ($n = 130$). Most of the adult surface-based parcellations performed no better than chance in neonatal data (Schaefer: $P = 0.771$, Glasser: $P = 0.012$, Gordon: $P = 0.658$) (Supplementary Fig. 4). While the Glasser et al. parcellation performed slightly better than chance, the z-score of 2.3 was much lower than z-scores typically reported for well-fitting parcellations in adults (Gordon et al. 2016). Surface-based parcellations from older infants (Wang 0-2Yr: $P = 0.188$, Wang 0-3Mo: $P = 0.247$) and neonate-specific volume-based parcellations (Scheinost: $P = 0.932$, Shi: $P = 1.000$) similarly did not perform better than chance in our surface-based neonatal data (Supplementary Fig. 4). Thus, neither surface-based parcellations derived from older samples nor volume-based parcellations derived from neonates adequately capture neonatal surface-based FC patterns, underscoring the need for a neonate-specific surface-based parcellation.

Neonatal boundary map

A neonatal boundary map was generated from the primary dataset ($n = 131$; Supplementary Table 1), identifying transitions in patterns of FC across the cortex (Fig. 1). Neonatal boundaries (Fig. 1A) appeared thicker and smoother compared to an adult dataset (Fig. 1B). Quantitatively, the spatial smoothness of the neonatal boundary map was 4.06 mm FWHM, compared to 3.2 mm FWHM for the adult group average boundary map, suggesting that the borders are less "sharp" in data averaged across neonates compared to data averaged across adults. In addition, we noted that smoothness of the neonatal boundary map increased with increasing number of neonates included in creating the average (Supplementary Fig. 5), suggesting that the smoothness of borders may result from variability in border placement across neonates. Consistent with this hypothesis, the spatial smoothness of a boundary map from an individual neonate (PB003) was 2.82 mm FWHM, comparable to the adult group average boundary map (Fig. 1C).

Neonatal parcel creation

The primary dataset (top half of participant in terms of data quality; $n = 131$) was split randomly into split-half 1 ($n = 65$) and split-half 2 ($n = 66$). Supplementary Table 2 shows demographic

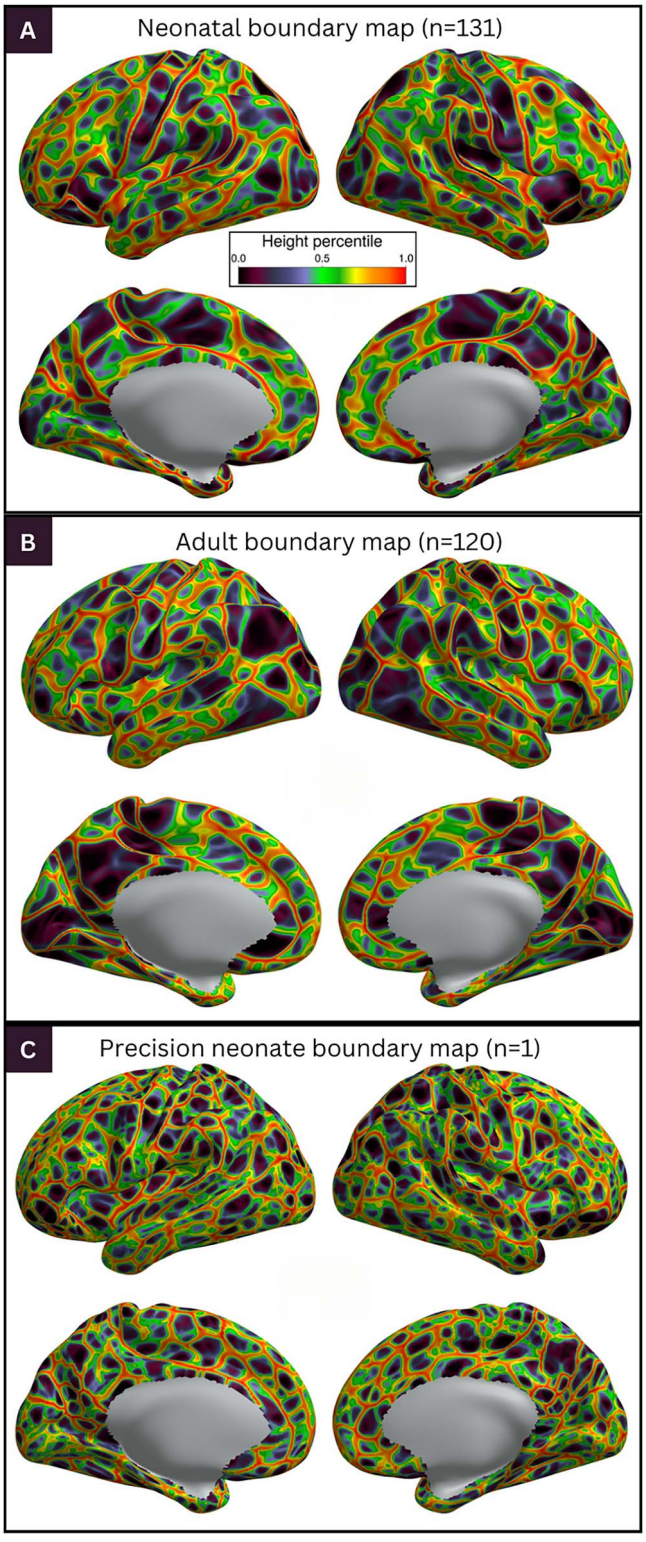

Fig. 1. *RSFC boundary maps generated based on abrupt changes in FC.* A) Neonatal RSFC boundary map generated based on the average of all 131 subjects' gradient maps. B) Adult RSFC boundary map based on the average of 120 subjects. C) Neonatal RSFC boundary map generated based on a single neonate's gradient maps. Boundaries are indicated by color based on height percentile of edge density, where bright colors indicate locations where abrupt transitions in RSFC patterns were consistent across many cortical vertices, and darker colors represent areas of cortex where the RSFC patterns were relatively stable.

information for each split half. For each split half, we created a separate boundary map (similar to Fig. 1A) and then generated a series of parcellations over a range of height criteria (from the 25th to the 90th percentile of height values). Figure 2A illustrates how each split-half parcellation performed at each height threshold against both its generating sample and the held-out sample. Parcellations performed extremely well when tested against the held-out sample ($z \sim 9$–10) at lower height thresholds (25th through 50th percentiles). Performance steadily declined as height criteria increased beyond an inflection point at the 50th percentile. Performance was lowest at the 90th percentile but still significantly better than chance for the held-out samples (z close to or above 3.3, $P < 0.001$). Thus, we concluded that the optimal height criteria for our neonatal parcellation in terms of generalizability and within-sample testing was 50%. Notably, parcellations derived from the 50% versus 90% height thresholds covered 48% versus 81% of the cortical surface, respectively. Also of note, parcels derived using data from a single individual subject at the 90% height threshold worked extremely well in held-out data from the same individual collected on a separate day ($z = 13.2$). This result suggests that the relatively poorer fit of the parcels derived using the 90% height threshold in the group data is likely due to averaging data across subjects rather than something inherent to neonatal data. For example, the poor fit of the 90% parcels in group-average data could be due to variation in the precise location of parcel boundaries across individuals (Supplementary Fig. 6).

Figure 2B illustrates the parcels generated from each split-half at the 50% height threshold. Parcels from split-half 1 are shown in blue, parcels from split-half 2 are shown in green, and areas of parcel overlap are colored cyan. Visual inspection of Fig. 2B indicates good overlap between the parcels generated from the two split halves across most of the cortical surface. The Dice coefficient of overlap in parcels from the two split halves was 0.69 and was highly significant based on rotation-based null models ($z = 19.5$).

Our "final" parcellation was generated from the primary dataset ($n = 131$) at the 50% height criterion and is shown in Fig. 3. There were 283 parcels in this final Myers-Labonte Parcellation, with 146 parcels in the left hemisphere and 137 in the right.

Neonatal parcellation has high homogeneity

The homogeneity value of each parcel in the final Myers-Labonte Parcellation is illustrated in Fig. 3A. Most generated parcels (red dots) had homogeneity values higher than expected by chance compared against random parcel rotations (black dots) on the cortical surface (Fig. 3C). As depicted in Fig. 3B, and as previously noted (Gordon et al. 2016), larger parcels tended to be less homogenous; however, larger parcels tended to do better against the null rotations compared to smaller parcels, due to smaller parcels having high homogeneity in many of the null rotations. The parcellation as a whole also had higher homogeneity averaged across all 283 parcels (Fig. 3C; red dot) compared against the average homogeneity from any of the 1,000 null rotations ($P < 0.001$) (Fig. 3C; black dots). The homogeneity of the real parcellation was 9.36 standard deviations above the mean of the null rotations.

Parcellation generated from neonatal data has high homogeneity in external datasets

The final Myers-Labonte neonatal parcellation was validated against three separate external neonatal datasets by comparing the average homogeneity across all parcels against average

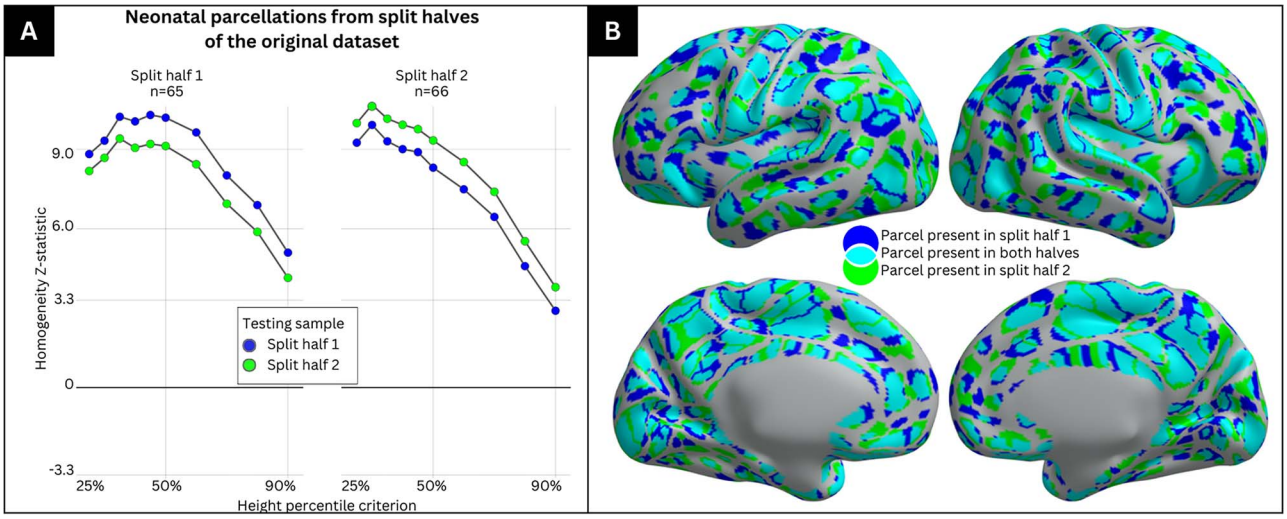

Fig. 2. *Parcels generated at the 50% height threshold from split halves of the primary dataset highly overlap with one another.* A) the primary dataset was split into split half 1 and split half 2 and used to generate parcellations at varying height thresholds between 25% and 90%. Each split-half parcellation was then tested against the sample that generated the parcellation and the other split half. The left panel represents the homogeneity z-statistic of the parcellation generated from split half 1 tested against itself (blue) and the other split half (green) at varying height thresholds. The right panel represents the homogeneity z-statistic of the parcellation generated from split half 2 tested against itself (green) and the other split half (blue) at varying height thresholds. B) Medial and lateral view of the right and left hemisphere showing parcels which are identified in split half 1 only (blue), split half 2 only (green) and in both split halves (cyan).

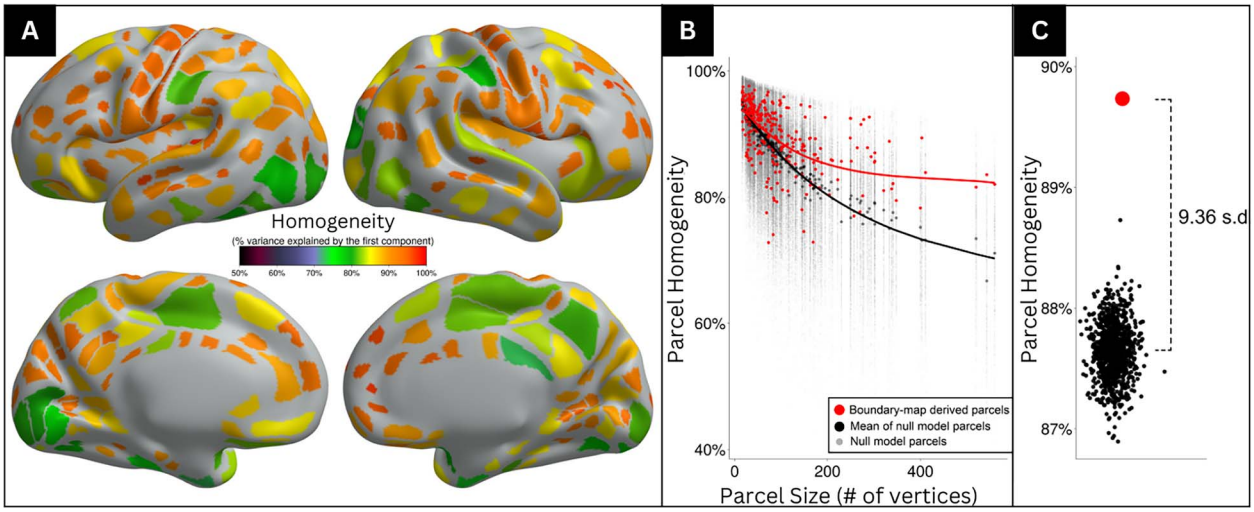

Fig. 3. *The parcellation generated from the primary dataset (n = 131) shows 283 highly homogenous parcels at 50% height threshold.* A) Parcels are colored based on homogeneity value, calculated based on percent variance explained by the first principal component of the connectivity patterns of the individual vertices comprising each parcel. B) the homogeneity of each parcel (red dots) is plotted as a function of parcel size. Black dots indicate the homogeneity of each parcel over 1,000 null rotations. Note that many parcels had true homogeneity values higher than the average of null rotations, especially larger parcels. C) the performance of the entire parcellation scheme tested against 1,000 null rotations. The black dots indicate the average homogeneity value across all 283 parcels for each of the 1,000 null rotations. The red dot represents the average homogeneity value across all 283 parcels in the true data. The average homogeneity across all parcels was 9.36 standard deviations above the mean of the null rotations.

homogeneity from 1,000 null rotations. In Fig. 4A, bars illustrate testing of the parcels against the excluded half of the dataset (the half of the dataset with lower amounts of retained data after censoring; $n = 130$) and against three different external datasets. The parcellation generated from the primary dataset performed very well against its excluded half ($z = 9.0$), the CUDDEL external group dataset ($z = 8.92$), and the precision dataset (PB003) from a single highly sampled neonate ($z = 6.55$). The parcellation also performed well against the older, single-band WUNDER dataset ($z = 3.22$). Parcels generated from the primary dataset at height thresholds other than 50% also outperformed chance in external datasets as illustrated in Supplementary Fig. 7. Parcellation homogeneity remained robust even in external datasets with small sample sizes (Supplementary Fig. 1).

As internal and external validation suggested that the neonatal parcellation performed best using a 50% height criterion, which was substantially different than the criterion previously used for the published adult parcellation [90%; (Gordon et al. 2016)], we also generated "Gordon parcels" at varying height thresholds (25%–90%) with our modified steps parameter ($n = 1,600$). We tested these "Gordon parcels" generated from different height thresholds against our neonatal dataset (Fig. 4B), and the adult-based parcels performed no better than chance in the primary neonatal dataset at every height threshold. We further tested the published "Gordon parcels" without any modifications (90%

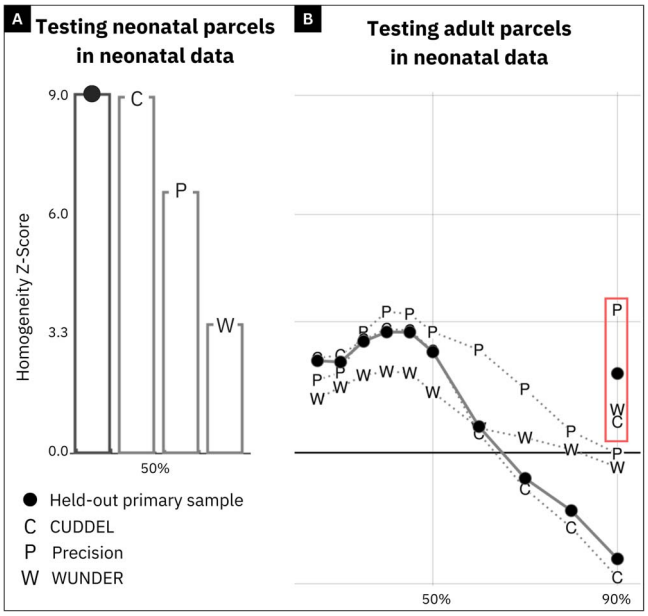

Fig. 4. *Validation of neonatal parcellations.* A) The primary dataset ($n = 131$) was used to generate a parcellation which was tested in four datasets. The bar graph represents the homogeneity z-statistic of the parcellation generated from the primary dataset against the second, held-out half of the dataset ($n = 130$; black dot) and three external datasets (CUDDEL+OXYGEN, C; precision baby, P; WUNDER, W). B) Adult "Gordon parcels" were generated using the same parameters as used in generating the neonatal parcels and were applied to the primary dataset (black dots), as well as external datasets (CUDDEL+OXYGEN, C; precision baby, P; WUNDER, W), to test the fit of adult parcels on the neonatal FC data across height thresholds (25–90%). Markers in the red rectangle denote testing of "Gordon parcels" with original published parameters (90% height threshold; $n = 400$ steps) on each neonatal dataset. Note that adult parcels do a poor job of capturing neonatal FC patterns.

height threshold; $n = 400$ steps) (Gordon et al. 2016) on our external neonatal datasets and found that these parcels also performed no better than chance. Thus, the improved fit of neonatal-generated as compared to adult-generated parcels on neonatal data are not due to the difference in the height threshold used to generate the parcels from the boundary map.

Network identities of parcels

We assigned functional network identities to each parcel using the Infomap algorithm. Figure 5 shows "consensus" networks obtained by using information across all edge densities. Supplementary Fig. 8 shows assigned network identities at a selection of edge densities (0.25–10%). Supplementary Table 3 lists all individual parcels by their associated ID number, consensus network assignment, and color in Fig. 5. Figure 6 shows a spring-embedded representation of the parcels and their network configuration across four representative edge densities. Together, Figs. 5 and 6 provide key insights into how neonatal parcels are organized into networks.

In general, parcels tended to group into networks reminiscent of anatomically isolated sub-portions of adult networks (i.e. most neonatal "networks" only included sets of physically adjacent parcels). For example, the four networks in shades of yellow (see Supplementary Table 3 for color names) each included only physically adjacent parcels, but together the four networks cover spatially distributed portions of cortex roughly corresponding to the adult fronto-parietal network (FPN). Similarly, the two networks in shades of red together cover portions of cortex roughly corresponding to the adult default mode network (DMN). Additional networks were identified similar to adult dorsal attention (DAN), ventral attention, salience, premotor, motor, visual, and auditory networks. Both the DAN and the posterior DMN included parcels distributed across cortex that were not physically adjacent. Notably, we did not identify a network that clearly corresponded to the cingulo-opercular network (CON); though we did identify several networks that we named based on anatomical location (e.g. cingulate network) that may correspond to sub-portions of the CON.

Spring-embedded representations (Fig. 6) are useful for examining within- and between- network relations of the entire parcellation. In such representations, stronger connections tend to pull parcels closer together, and so the proximity of parcels to each other is related to their inter-connectivity. Spring-embedded representations can be drawn when considering different edge densities, i.e. considering only the strongest functional connections (low edge densities) or considering progressively weaker functional connections (higher edge densities).

The spring-embedded plots reveal that at sparse edge densities that include only the strongest functional connections, parcels cluster by network (color) and then by proximity on the cortical surface (frontal vs. posterior cortex). At the 4% edge density, for example, the frontal lobe networks are in close proximity to each other with few connections to the posterior networks. At denser edge densities, however, (e.g. 10%), there are more functional connections between frontal and posterior parcels, with some selectivity in these connections based on adult network properties. For example, the neonatal networks that putatively correspond to the posterior and anterior portions of the adult-DMN seem to draw together at denser edge densities, as do the posterior and anterior portions of the adult-FPN.

The neonatal connectivity matrix (Supplementary Fig. 9) also reflected the nascent features of adult-like organization. For example, the motor networks were all positively correlated with each other but negatively correlated with parcels from remaining networks, and the two halves of the putative DMN showed positive correlation with each other.

Discussion

The current study generated a set of 283 highly homogeneous, reproducible, and externally validated parcels on the cortical surface of the neonatal brain (Myers-Labonte Parcellation). Parcels from the published literature generated in surface-space from older infants and adults, as well as in volume-space parcels in neonates, in contrast, provided a poor fit to surface-based neonatal data. The boundaries denoting transitions in group-average neonatal connectivity between homogeneous parcels were thicker and smoother compared to adult datasets, possibly due to heterogeneity across neonates in the exact placement of parcel borders. As a result, the most generalizable results were obtained when restricting parcels to cover 50% of the neonatal cortical surface. This neonatal parcellation showed high validity both within-sample and across three external datasets, including neonates with a large range of socioeconomic backgrounds and in-utero drug exposure. Network assignments derived for the neonatal parcels were consistent with prior work: "networks" consisted largely of anatomically adjacent clusters of parcels, but specific sets of neonatal networks together covered anatomical territory reminiscent of adult networks.

Adult and older infant parcellations do not fit neonatal data

Surface-based adult and older-infant brain parcellations, as well as neonate-specific volume-based brain parcellations, generally

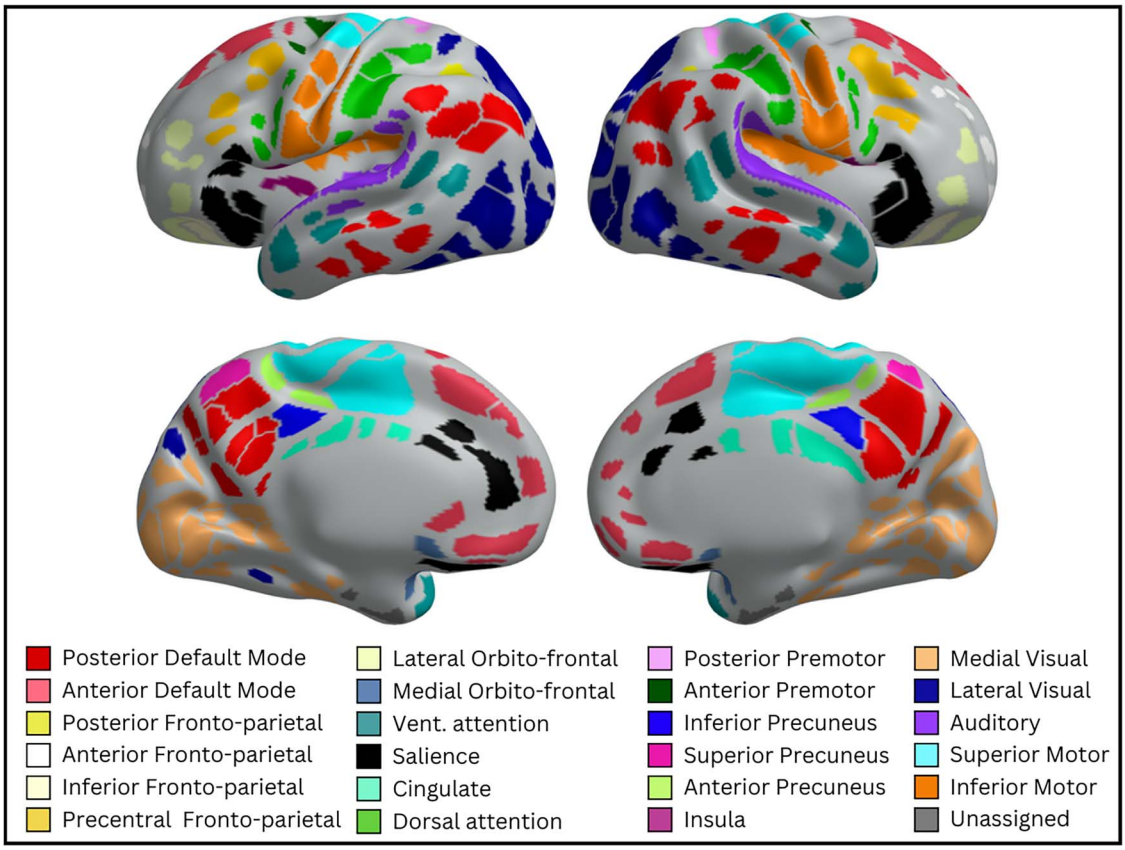

Fig. 5. *Assigned functional network identities for each parcel.* Consensus network assignments for each parcel based on information across all edge densities. Colors and network names were assigned based on adult networks in similar anatomical locations.

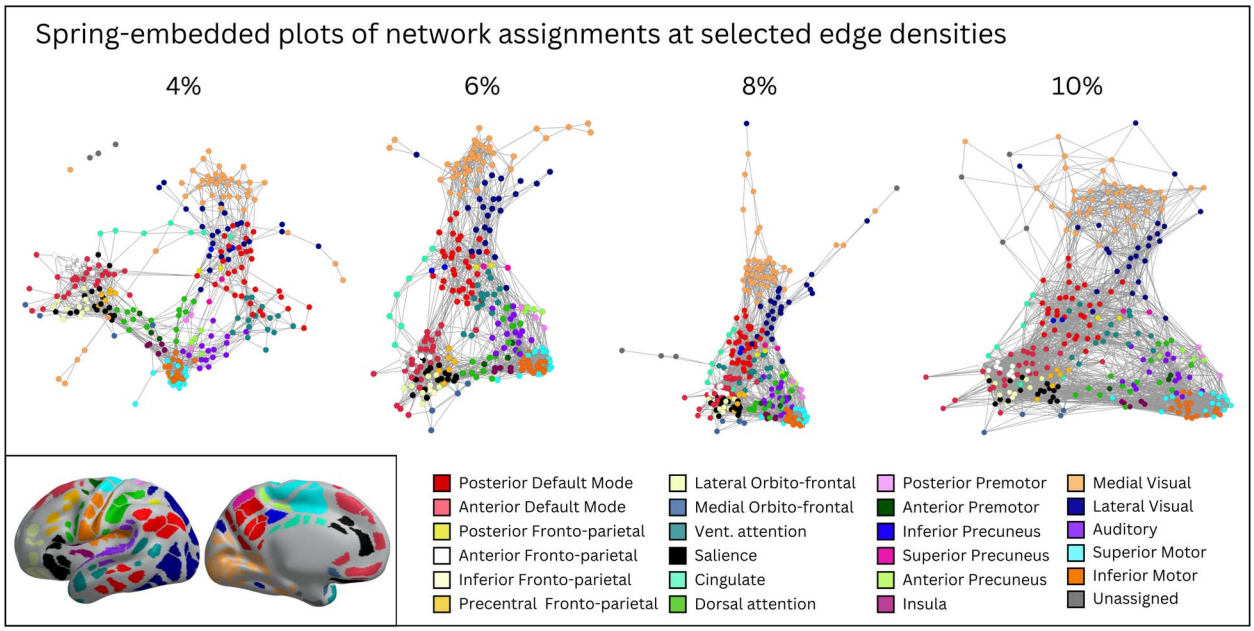

Fig. 6. *Spring-embedded plots of neonatal parcels across different edge densities reveal neonatal network properties.* A spring-embedded layout of neonatal functional connections at various edge densities between 4% and 10%. Each colored circle corresponds to a particular parcel, colored based on consensus network assignment. Lines represent functional connections between parcels at a given edge density (e.g. at 4% edge density, only the top 4% of positive functional connections are shown). In the spring-embedded representation, stronger connections tend to pull parcels closer together, and so the proximity of parcels to each other is related to their inter-connectivity. Note that when only considering the strongest connections (e.g. 4%), parcels cluster mainly by network (color) and anatomical location (e.g. frontal networks are all near each other); but when considering weaker connections (e.g. 10%), there is some evidence of selective connections between anatomically distant parcels that end up forming the same adult network (e.g. the red and watermelon parcels draw close to each other; these parcels may be precursors of the adult default mode network). Inset shows consensus network assignment of each parcel for reference (identical to Fig. 5).

performed no better than chance in neonatal data, emphasizing the need for a neonate-specific surface-based parcellation. The neonatal brain is about one-fourth the size of the adult brain, and expansion of the cortical surface over development is non-linear and non-uniform (Hill et al. 2010; Li et al. 2013). This non-uniform expansion is the most likely explanation for the poor fit of adult and older-infant surface-based parcels on neonatal data. Volume-derived neonatal parcellations also provided a poor fit for neonatal surface FC data, likely because volume-derived parcels can combine portions of cortex that are near to each other in volume-space but more distant in surface-space (such as tips of physically adjacent gyri). For this reason, surface-derived parcels may provide more biologically plausible candidates for cortical areas than volume-derived parcels.

A consequence of the results described above is that neonatal neuroimaging studies using surface-based representations should use neonatally derived surface parcellations such as the currently presented Myers-Labonte parcellation. Surface-based infant/adult parcels and volume-based neonatal parcels will not capture functionally homogenous portions of cortex in surface-based neonatal data. The problem with using poorly fitting parcels is that they will mix signals from cortical areas with different functional properties. Work in adults and older infants demonstrates that studies using such poorly fitting parcels are less likely, in general, to detect brain-behavior relations (Wang et al. 2018; Kong et al. 2021). Studies that do detect brain-behavior relations using poorly fitting parcels would be more difficult to interpret, because they are mixing signals from more than one biologically relevant subdivision of the brain.

Neonatal boundaries between parcels are thicker and smoother than in adults in group-average data

The zones of transition in FC patterns across the cortical surface, or "boundaries" were thicker and smoother in group-average neonatal datasets compared to adults. Because the boundary smoothness of an *individual* neonate was comparable to that of adults and parcels generated in an *individual* neonate were highly homogenous and reliable even at the 90% height threshold, the most likely explanation of this difference is greater variation across different neonates in exact placement of boundaries. This hypothesis is further supported by the observation that measured border smoothness increased with the number of neonates included in the average. The most likely explanation for increased variability of neonatal boundaries is that the neonatal period is a time of rapid development (Nielsen et al. 2022). As a result, differences in structural development (e.g. cortical folding, surface area) make it more difficult to obtain precise registration of functional data across neonates even with surface registration (Wang et al. 2023). A practical consequence is that parcellations that cover large portions of the neonatal brain (e.g. 90%) include portions of the thick boundaries and thus do not provide as good of a fit to good average data as parcellations that are restricted to the wells between the thick boundaries (e.g. the parcellation generated using the 50% height threshold). While we make both the 90% and 50% height threshold parcellations publicly available, we recommend use of the version generated at 50% because these parcels are demonstrated to be highly valid in external datasets. The parcellation generated from the 90% height threshold may be useful to researchers interested in studying variation across individuals or areas of the brain undergoing rapid development.

Neonatal parcels can be grouped into functional networks

Functional networks are sets of cortical areas that have high interconnectivity and have shared functional properties (Petersen and Sporns 2015). Functional networks thus represent an important organizational property of the human brain. In the current study, we used the Infomap algorithm to assign each neonatal parcel to a functional brain network, to aid studies that want to contextualize results by network. Consistent with prior work in neonates, empirically derived "networks" in neonates consisted largely of clusters of anatomically adjacent parcels and sets of these networks together comprised the approximate anatomical locations of anatomically distributed adult-like networks. For example, four of the neonatal networks combined together resembled the adult FPN and two of the neonatal networks combined resembled the adult DMN. Spring-embedded representations suggested that there was weak but selective FC between distinct neonatal networks that putatively combined later in development to be a single network, consistent with prior work (Doria et al. 2010; Smyser et al. 2010, 2016; Keunen et al. 2017; Molloy and Saygin 2022; Sylvester et al. 2022). An important goal of future work is to track how network organizational properties change over development.

Neonatal parcels provide an important foundation for studies of human brain development

The neonatal period is a critical stage in neural development that serves as a starting point for postnatal experience-dependent learning (Rai et al. 2022). Complex human behaviors are posited to depend on a tightly coordinated sequence of brain development that extends from the in-utero period through at least early adulthood (Tierney and Nelson 3rd. 2009). Many brain illnesses, including many psychiatric and neurological disorders, are thought to have their origin in very early brain development (Sylvester et al. 2018, 2021; Fleiss et al. 2019). Thus, characterizing neonatal cortical brain areas and their functional network characteristics is an important goal for systems neuroscience investigations into typical and atypical development. Parcels in the current study may represent cortical areas and thus provide an important starting point for characterizing human brain development.

Limitations

The present study should be viewed considering its limitations. As noted throughout, biological and methodological challenges may make it more difficult to functionally align groups of neonates compared to older samples using purely anatomical landmarks (i.e. surface-based registration). Consistent with this interpretation, some prior work in older infants has used functional brain properties to improve functional alignment across individuals (Wang et al. 2023). We chose not to incorporate functional alignment in the current study so that the derived parcels would be most generalizable for future neonatal neuroimaging studies, where in most cases it will be impractical to include functional alignment. The presented surface-based neonatal parcellation only includes a parcellation of the cortical surface and does not include subcortical brain structures. Parcellation of the subcortex was excluded from the Myers-Labonte parcellation because the surface-based approach used in the current study is not relevant to subcortical structures, i.e. relevant units of processing in the subcortex are more naturally captured by volumes. The proposed Myers-Labonte cortical surface parcellation could be combined

with other publicly available volume-based functional parcellations which include subcortical structures (Scheinost et al. 2016; Shi et al. 2017) or by utilizing publicly available structural divisions from tools like MCRIB (Adamson et al. 2020) for those interested in extending their analyses to include subcortical and cerebellar structures. Both the primary dataset and two of the external datasets were collected on Siemens Prisma 3T scanners, and a third validation dataset was collected on an older Siemens Trio; future work is required to determine how well the generated parcels fits data acquired on other scanners. All neonatal data in the current study were collected during natural sleep. While sleep state impacts some properties of FC in adults (Tagliazucchi and Laufs 2014), it is not known whether sleep state impacts the abrupt changes in FC that are used to define the borders of the parcels presented in the current paper. In theory, the location of cortical areas should not depend on sleep state, but it remains unknown whether sleep state impacts the measure used in the current paper to operationally define cortical areas. Future work should ascertain how well the parcels fit functional data from awake neonates. Finally, our neonates ranged in age from 38 to 45 wk PMA, and additional work is required to determine the specific ages in which it is most appropriate to use these parcels.

Conclusion

We generated a highly reliable set of 283 surface-based parcels for the neonatal brain that were validated using three external datasets. We additionally provide functional brain network assignments for each parcel. This parcellation will aid neonatal neuroimaging studies that seek to describe results contextualized by functionally relevant cortical areas.

Acknowledgments

We thank the families of all of our participants from these studies for their participation and dedication toward research.

Author contributions

Michael J. Myers (Conceptualization, Data curation, Formal analysis, Methodology, Software, Visualization, Writing—original draft), Alyssa Labonte (Formal analysis, Visualization, Writing—original draft, Writing—review & editing), Evan M. Gordon (Methodology, Writing—review & editing), Timothy Laumann (Methodology, Writing—review & editing), Jiaxin Cindy Tu (Formal analysis, Methodology, Visualization, Writing—review & editing), Muriah Wheelock (Writing—review & editing), Ashley N. Nielsen (Writing—review & editing), Rebecca F. Schwarzlose (Writing—review & editing), M Catalina Camacho (Writing—review & editing), Dimitrios Alexopoulos (Data curation), Barbara B. Warner (Funding acquisition, Resources), Nandini Raghuraman (Funding acquisition, Resources), Joan L. Luby (Funding acquisition, Resources), Deanna M. Barch (Funding acquisition, Resources), Damien A. Fair (Methodology, Resources), Steven E. Petersen (Methodology, Writing—review & editing), Cynthia E. Rogers (Funding acquisition, Resources, Writing—review & editing), Christopher D. Smyser (Funding acquisition, Resources, Writing—review & editing), and Chad M. Sylvester (Conceptualization, Funding acquisition, Resources, Supervision, Writing—original draft)

Supplementary material

Supplementary material is available at *Cerebral Cortex* online.

Funding

This work was supported by funds provided by the Intellectual and Developmental Disabilities Research Center at Washington University (P50 HD103525); the Taylor Family Foundation; the Washington University in St. Louis March of Dimes Prematurity Research Center; the National Institute of Mental Health (R01MH122389, R01MH131584); the National Institute on Drug Abuse (R01DA046224, U24DA055330); and the National Institute of Child Health and Human Development (K99HD109454).

Conflict of interest statement: Damien A. Fair is a patent holder on the Framewise Integrated Real-Time Motion Monitoring (FIRMM) software. He is also a co-founder of Turing Medical Inc. that licenses this software. The nature of this financial interest and the design of the study have been reviewed by the University of Minnesota, and a plan has been established to ensure that this research study is not affected by the financial interest. The other authors declare no competing interests.

Data availability

The derived parcellation (Myers-Labonte Parcellation) and the code used to derive the parcels in this work are publicly available at https://github.com/myersm0/myers-labonte_parcellation/. Based on the results above, for typical group studies of neonates, we recommend use of the parcels at 50% height threshold, as depicted in Fig. 3 and Fig. 5. These parcels are expected to be highly valid across different datasets and individuals, while still covering a substantial portion of the cortical surface. We also make available the parcels across a range of other height thresholds, including the 90% threshold that covers 81% of the cortical surface (Supplementary Fig. 10); but note that these parcels are not expected to be as valid across all datasets and subjects. Parcels in the available dataset are numbered according to Supplementary Table 3, which also includes network identification. Supplementary Fig. 11 shows each parcel labeled with its parcel number and network identification. All original code has been deposited at https://github.com/myersm0/WatershedParcellation.jl/ and is publicly available. All data reported in this paper will be shared by the corresponding author upon request as per study governance procedures.

References

Adamson CL, Alexander B, Ball G, Beare R, Cheong JLY, Spittle AJ, Doyle LW, Anderson PJ, Seal ML, Thompson DK. Parcellation of the neonatal cortex using surface-based Melbourne Children's regional infant brain atlases (M-CRIB-S). *Sci Rep*. 2020:10(1):4359.

Alexander B, Murray AL, Loh WY, Matthews LG, Adamson C, Beare R, Chen J, Kelly CE, Rees S, Warfield SK, et al. A new neonatal cortical and subcortical brain atlas: the Melbourne Children's regional infant brain (M-CRIB) atlas. *NeuroImage*. 2017:147:841–851.

Arslan S, Ktena SI, Makropoulos A, Robinson EC, Rueckert D, Parisot S. Human brain mapping: a systematic comparison of parcellation methods for the human cerebral cortex. *NeuroImage*. 2018:170:5–30.

Badke, D'Andrea C, Kenley JK, Montez DF, Mirro AE, Miller RL, Earl EA, Koller JM, Sung S, Yacoub E, Elison JT, et al. Real-time motion monitoring improves functional MRI data quality in infants. *Dev Cogn Neurosci*. 2022:55:101116.

Beucher S, Lantuejoul C. *Use of watersheds in contour detection. Presented at the international workshop on image processing: real-time edge and motion detection/estimation*. Rennes, France, 1979.

Cohen AL, Fair DA, Dosenbach NUF, Miezin FM, Dierker D, Van Essen DC, Schlaggar BL, Petersen SE. Defining functional areas in individual human brains using resting functional connectivity MRI. *NeuroImage*. 2008:41(1):45–57.

Danisch S, Krumbiegel J. Makie.jl: flexible high-performance data visualization for Julia. *J Open Source Softw*. 2021:6(65):3349.

De Asis-Cruz J, Bouyssi-Kobar M, Evangelou I, Vezina G, Limperopoulos C. Functional properties of resting state networks in healthy full-term newborns. *Sci Rep*. 2015:5(1):1–15.

Doria V, Beckmann CF, Arichi T, Merchant N, Groppo M, Turkheimer FE, Counsell SJ, Murgasova M, Aljabar P, Nunes RG, et al. Emergence of resting state networks in the preterm human brain. *Proc Natl Acad Sci USA*. 2010:107(46):20015–20020.

Dosenbach NUF, Koller JM, Earl EA, Miranda-Dominguez O, Klein RL, Van AN, Snyder AZ, Nagel BJ, Nigg JT, Nguyen AL, et al. Real-time motion analytics during brain MRI improve data quality and reduce costs. *NeuroImage*. 2017:161:80–93.

Felleman DJ, Van Essen DC. Distributed hierarchical processing in the primate cerebral cortex. *Cereb Cortex*. 1991:1(1):1–47.

Fleiss B, Rivkees SA, Gressens P. Early origins of neuropsychiatric disorders. *Pediatr Res*. 2019:85(2):113–114.

Fransson P, Skiöld B, Horsch S, Nordell A, Blennow M, Lagercrantz H, Aden U. Resting-state networks in the infant brain. *Proc Natl Acad Sci USA*. 2007:104(39):15531–15536.

Fransson P, Skiöld B, Engström M, Hallberg B, Mosskin M, Aden U, Lagercrantz H, Blennow M. Spontaneous brain activity in the Newborn brain during natural sleep—an fMRI study in infants born at full term. *Pediatr Res*. 2009:66(3):301–305.

Gao W, Zhu H, Giovanello KS, Smith JK, Shen D, Gilmore JH, Lin W. Evidence on the emergence of the brain's default network from 2-week-old to 2-year-old healthy pediatric subjects. *Proc Natl Acad Sci USA*. 2009:106(16):6790–6795.

Gao W, Gilmore JH, Shen D, Smith JK, Zhu H, Lin W. The synchronization within and interaction between the default and dorsal attention networks in early infancy. *Cereb Cortex*. 2013:23(3):594–603.

Gao W, Alcauter S, Elton A, Hernandez-Castillo CR, Smith JK, Ramirez J, Lin W. Functional network development during the first year: relative sequence and socioeconomic correlations. *Cereb Cortex*. 2015:25(9):2919–2928.

Gao W, Lin W, Grewen K, Gilmore JH. Functional connectivity of the infant human brain: plastic and modifiable. *Neuroscientist*. 2017:23(2):169–184.

Glasser MF, Sotiropoulos SN, Wilson JA, Coalson TS, Fischl B, Andersson JL, Xu J, Jbabdi S, Webster M, Polimeni JR, et al. The minimal preprocessing pipelines for the human connectome project. *NeuroImage*. 2013:80:105–124.

Glasser MF, Coalson TS, Robinson EC, Hacker CD, Harwell J, Yacoub E, Ugurbil K, Andersson J, Beckmann CF, Jenkinson M, et al. A multi-modal parcellation of human cerebral cortex. *Nature*. 2016:536(7615):171–178.

Gordon EM, Laumann TO, Adeyemo B, Huckins JF, Kelley WM, Petersen SE. Generation and evaluation of a cortical area Parcellation from resting-state correlations. *Cereb Cortex*. 2016:26(1):288–303.

Gordon EM, Laumann TO, Gilmore AW, Newbold DJ, Greene DJ, Berg JJ, Ortega M, Hoyt-Drazen C, Gratton C, Sun H, et al. Precision functional mapping of individual human brains. *Neuron*. 2017:95(4):791–807.e7.

Han L, Savalia NK, Chan MY, Agres PF, Nair AS, Wig GS. Functional Parcellation of the cerebral cortex across the human adult lifespan. *Cereb Cortex*. 2018:28(12):4403–4423.

Herzmann CS, Snyder AZ, Kenley JK, Rogers CE, Shimony JS, Smyser CD. Cerebellar functional connectivity in term- and very preterm-born infants. *Cereb Cortex*. 2019:29(3):1174–1184.

Hill J, Inder T, Neil J, Dierker D, Harwell J, Van Essen D. Similar patterns of cortical expansion during human development and evolution. *Proc Natl Acad Sci USA*. 2010:107(29):13135–13140.

Keunen K, Counsell SJ, Benders MJNL. The emergence of functional architecture during early brain development. *NeuroImage*. 2017:160:2–14.

Kong R, Yang Q, Gordon E, Xue A, Yan X, Orban C, Zuo X-N, Spreng N, Ge T, Holmes A, et al. Individual-specific areal-level Parcellations improve functional connectivity prediction of behavior. *Cereb Cortex*. 2021:31(10):4477–4500.

Laumann TO, Gordon EM, Adeyemo B, Snyder AZ, Joo SJ, Chen M-Y, Gilmore AW, McDermott KB, Nelson SM, Dosenbach NUF. Functional system and areal organization of a highly sampled individual human brain. *Neuron*. 2015:87(3):657–670.

Lean RE, Smyser CD, Brady RG, Triplett RL, Kaplan S, Kenley JK, Shimony JS, Smyser TA, Miller JP, Barch DM, et al. Prenatal exposure to maternal social disadvantage and psychosocial stress and neonatal white matter connectivity at birth. *Proc Natl Acad Sci USA*. 2022:119(42):e2204135119.

Li G, Nie J, Wang L, Shi F, Lin W, Gilmore JH, Shen D. Mapping region-specific longitudinal cortical surface expansion from birth to 2 years of age. *Cereb Cortex*. 2013:23(11):2724–2733.

Marcus DS, Harwell J, Olsen T, Hodge M, Glasser MF, Prior F, Jenkinson M, Laumann T, Curtiss SW, Van Essen DC. Informatics and data mining tools and strategies for the human connectome project. *Front Neuroinform*. 2011:5:4.

Marcus DS, Harms MP, Snyder AZ, Jenkinson M, Wilson JA, Glasser MF, Barch DM, Archie KA, Burgess GC, Ramaratnam M, et al. Human connectome project informatics: quality control, database services, and data visualization. *NeuroImage*. 2013:80:202–219.

Mathur AM, Neil JJ, McKinstry RC, Inder TE. Transport, monitoring, and successful brain MR imaging in unsedated neonates. *Pediatr Radiol*. 2008:38(3):260–264.

Molloy MF, Saygin ZM. Individual variability in functional organization of the neonatal brain. *NeuroImage*. 2022:253:119101.

Nepusz GCA. The igraph software package for complex network research. *InterJournal Complex Syst*. 2006:1695.

Nielsen AN, Kaplan S, Meyer D, Alexopoulos D, Kenley JK, Smyser TA, Wakschlag LS, Norton ES, Raghuraman N, Warner BB, et al. Maturation of large-scale brain systems over the first month of life. *Cereb Cortex*. 2022:33(6):2788–2803.

Ojemann JG, Akbudak E, Snyder AZ, McKinstry RC, Raichle ME, Conturo TE. Anatomic localization and quantitative analysis of gradient refocused echo-planar fMRI susceptibility artifacts. *NeuroImage*. 1997:6(3):156–167.

Petersen SE, Sporns O. Brain networks and cognitive architectures. *Neuron*. 2015:88(1):207–219.

Power JD, Cohen AL, Nelson SM, Wig GS, Barnes KA, Church JA, Vogel AC, Laumann TO, Miezin FM, Schlaggar BL, et al. Functional network organization of the human brain. *Neuron*. 2011:72(4):665–678.

Power JD, Mitra A, Laumann TO, Snyder AZ, Schlaggar BL, Petersen SE. Methods to detect, characterize, and remove motion artifact in resting state fMRI. *NeuroImage*. 2014:84:320–341.

Rai B, Seidlitz J, White SR, Vogel JW, Anderson KM, Adamson C, Adler S, Alexopoulos GS, Anagnostou E, Areces-Gonzalez A, et al. Brain charts for the human lifespan. *Nature*. 2022:604(7906):525–533.

Rosvall M, Bergstrom CT. Maps of random walks on complex networks reveal community structure. *Proc Natl Acad Sci USA*. 2008:105(4):1118–1123.

Schaefer A, Kong R, Gordon EM, Laumann TO, Zuo X-N, Holmes AJ, Eickhoff SB, Yeo BTT. Local-global Parcellation of the human cerebral cortex from intrinsic functional connectivity MRI. *Cereb Cortex*. 2018:28(9):3095–3114.

Scheinost D, Kwon SH, Shen X, Lacadie C, Schneider KC, Dai F, Ment LR, Constable RT. Preterm birth alters neonatal, functional rich club organization. *Brain Struct Funct*. 2016:221(6):3211–3222.

Sejnowski TJ, Churchland PS. 1989. Brain and cognition. In: Posner MI, editor. *Foundations of cognitive science* , (pp. Cambridge, MA, US: The MIT Press, xiv. p. 301–356.

Shi F, Salzwedel AP, Lin W, Gilmore JH, Gao W. Functional brain Parcellations of the infant brain and the associated developmental trends. *Cereb Cortex*. 2017:28(4):1358–1368.

Shine JM, Breakspear M, Bell PT, Ehgoetz Martens KA, Shine R, Koyejo O, Sporns O, Poldrack RA. Human cognition involves the dynamic integration of neural activity and neuromodulatory systems. *Nat Neurosci*. 2019:22(2):289–296.

Smyser CD, Inder TE, Shimony JS, Hill JE, Degnan AJ, Snyder AZ, Neil JJ. Longitudinal analysis of neural network development in preterm infants. *Cereb Cortex*. 2010:20(12):2852–2862.

Smyser CD, Snyder AZ, Shimony JS, Mitra A, Inder TE, Neil JJ. Resting-state network complexity and magnitude are reduced in prematurely born infants. *Cereb Cortex*. 2016:26(1):322–333.

Sydnor VJ, Larsen B, Bassett DS, Alexander-Bloch A, Fair DA, Liston C, Mackey AP, Milham MP, Pines A, Roalf DR, et al. Neurodevelopment of the association cortices: patterns, mechanisms, and implications for psychopathology. *Neuron*. 2021:109(18):2820–2846.

Sylvester CM, Smyser CD, Smyser T, Kenley J, Ackerman JJ Jr, Shimony JS, Petersen SE, Rogers CE. Cortical functional connectivity evident after birth and Behavioral inhibition at age 2. *Am J Psychiatry*. 2018:175(2):180–187.

Sylvester CM, Myers MJ, Perino MT, Kaplan S, Kenley JK, Smyser TA, Warner BB, Barch DM, Pine DS, Luby JL, et al. Neonatal brain response to deviant auditory stimuli and relation to maternal trait anxiety. *Am J Psychiatry*. 2021:178(8):771–778.

Sylvester CM, Kaplan S, Myers MJ, Gordon EM, Schwarzlose RF, Alexopoulos D, Nielsen AN, Kenley JK, Meyer D, Yu Q, et al. Network-specific selectivity of functional connections in the neonatal brain. *Cereb Cortex*. 2022:33(5):2200–2214.

Tagliazucchi E, Laufs H. Decoding wakefulness levels from typical fMRI resting-state data reveals reliable drifts between wakefulness and sleep. *Neuron*. 2014:82(3):695–708.

Talairach J, Tournoux P. *Co-planar stereotaxic atlas of the human brain: 3-dimensional proportional system: an approach to cerebral imaging*. Stuttgart, Germany: Thieme Publishing Group; 1988.

Tierney AL, Nelson CA 3rd. Brain development and the role of experience in the early years. *Zero Three*. 2009:30(2):9–13.

van den Heuvel MP, Kersbergen KJ, de Reus MA, Keunen K, Kahn RS, Groenendaal F, de Vries LS, Benders MJNL. The neonatal connectome during preterm brain development. *Cereb Cortex*. 2015:25(9):3000–3013.

Wang D, Li M, Wang M, Schoeppe F, Ren J, Chen H, Öngür D, Brady RO, Baker JT, Liu H. Individual-specific functional connectivity markers track dimensional and categorical features of psychotic illness. *Mol Psychiatry*. 2018:25(9):2119–2129.

Wang F, Zhang H, Wu Z, Hu D, Zhou Z, Girault JB, Wang L, Lin W, Li G. Fine-grained functional parcellation maps of the infant cerebral cortex. *elife*. 2023:12:e75401.

Wig GS, Schlaggar BL, Petersen SE. Concepts and principles in the analysis of brain networks. *Ann N Y Acad Sci*. 2011:1224(1):126–146.

Wig GS, Laumann TO, Petersen SE. An approach for parcellating human cortical areas using resting-state correlations. *NeuroImage*. 2014:93(Pt 2):276–291.